Crystallization and structure analysis of the core motif of the Pks13 acyltransferase domain from *Mycobacterium tuberculosis*

Mingjing Yu [1], **Chao Dou** [1], **Yijun Gu** [2], **Wei Cheng** Corresp. [1]

[1] Department of Respiratory and Critical Care Medicine, West China Hospital, Sichuan University, Chengdu, Sichuan, People's Republic of China

[2] National Center for Protein Science, Shanghai, People's Republic of China

Corresponding Author: Wei Cheng
Email address: chwlab@163.com

Type I polyketide synthase 13 (Pks13) is involved in the final step of the biosynthesis of mycolic acid in *Mycobacterium tuberculosis* (Mtb). Recent articles have reported that Pks13 is an essential enzyme in the mycolic acid biosynthesis pathway, and it has been deeply studied as a drug target in TB. Here, we report a high-resolution structure of the acyltransferase (AT) domain of Pks13 at 2.59 Å resolution. Structural comparison with the full-length AT domain (PDB code, 3tzw and 3tzz) reveals a different orientation of the C-terminal helix.

Crystallization and structure analysis of the core motif of the Pks13 acyltransferase domain from *Mycobacterium tuberculosis*

Mingjing Yu[a], Chao Dou[a], Yijun Gu[b] and Wei Cheng[a]*

a Department of Respiratory and Critical Care Medicine, West China Hospital, Sichuan University, 37 Guoxue Road, Chengdu, Sichuan, 610041, People's Republic of China

b National Center for Protein Science Shanghai China, People's Republic of China

*Correspondence email: cwlab@163.com

Abstract

Type I polyketide synthase 13 (Pks13) is involved in the final step of the biosynthesis of mycolic acid in Mycobacterium tuberculosis (Mtb). Recent articles have reported that Pks13 is an essential enzyme in the mycolic acid biosynthesis pathway, and it has been deeply studied as a drug target in TB. We report a high-resolution structure of the acyltransferase (AT) domain of Pks13 at 2.59 Å resolution. Structural comparison with the full-length AT domain (PDB code, 3tzw and 3tzz) reveals a different orientation of the C-terminal helix.

Introduction

Tuberculosis (TB) and its drug-resistant forms are still primary causes of mortality surpassing other infectious diseases **(WHO, 2015)**, emphasizing the unmet clinical need for new drugs with novel mechanisms**.** Owing to the indispensable and specific lipids forming the envelope of Mtb (**Dubnau et al., 2000**), targeting the synthesis and transport pathways of mycolic acids has always been a main route of TB drug discovery **(North et al., 2014; Wilson et al., 2013; Brennan et al., 1995; Bhatt et al., 2007**).

Recently, powerful evidence has verified that Pks13 is an essential enzyme in the mycolic acid biosynthesis pathway **(Gavalda et al., 2009; Portevin et al., 2016)**, and it has been deeply studied as a drug target in TB **(Aggarwal et al., 2017; Thanna et al., 2016)**. The type-1 polyketide synthase

enzyme Pks13 consists of five domains. The medial three are mandatory PKS domains, namely, the ketoacylsynthase (KS) domain, the AT domain and the acyl carrier protein (ACP) domain. The other ACP domain is adjacent to the KS domain, and the thioesterase (TE) domain is the C-terminal of Pks13. The overall Pks13 topological structure has the order ACP-KS-AT-ACP-TE (Fig. 1A).

The residue Ser55 in the N-ACP domain has been identified as a very important active site for initializing the pathway. Phosphopantetheinyl (P-pant) transferase (PPtT), encoded by the sfp gene, modifies the ACPs by providing a P-pant arm for the general function of carrying the substrate acyl chain via a thioester bond involving its terminal thiol group (**Wilson et al., 2013; Gavalda et al., 2009; Chalut et al., 2006**). The meromycoloyl on the N-ACP domain is transferred to the KS domain, and the intermediate product α-alkyl β-ketothioester is produced by a Claisen-type condensation reaction with another substrate carboxyacyl-CoA loaded by the AT domain. The mycolic acid precursor generated by the C-terminal ACP domain is then released by the TE domain (**Abrahams et al., 2016; Dubey et al., 2002**).

Despite increasing insights into the mechanism of Pks13, no full-length structural information has yet been reported, although some domain structures have been solved (**Herbst et al., 2016; Bergeret et al., 2012**).

Here, we report a high-resolution structure of the core motif of the AT domain. At first, the full-length Pks13 protein was successfully purified and we perform an extended crystal screening, in which the initial crystal was obtained. During the process of attempting to phase the diffraction data of the crystal, we found that the crystalized protein directing to a degraded one. The N-terminal sequence based on mass spectrum was performed, coinciding with the Se-Met crystal dataset, to confirm that the crystal was actually degraded (717 aa to 826 aa) (Fig. 1B). The crystal structure displays a similar overall fold to that of the reported AT domain (PDB code 3tzw), but the C-terminal end of the helix orientation is slightly different.

We believe that the comprehensive structural studies of Pks13 will pave the way for structure-based anti-mycobacterial drug design and drug screening.

Materials & Methods

Cloning, Over-expression, and Purification

The codon-optimized gene encoding the Pks13 full-length protein originating from *Mycobacterium tuberculosis* was ligated into the *Nde* I and *Xho* I sites of the pET-28b expression plasmid (Novagen, Madison, WI, USA). The sfp gene from *Bacillus subtilis* str.168 **(Chalut et al., 2006)**, which encodes the 4 -phosphopantetheinyl (P-pant) transferase PptT that serves as a kind of co-factor to modify Ser55 in the N-ACP domain of Pks13, was also ligated into the *Nde* I and *Xho* I sites of the pET-21b expression plasmid (Novagen, Madison, WI, USA), and a terminator codon was added in the C-terminal end. The detailed information on these constructs is shown in Table 1. All constructed plasmids were verified by sequencing.

The constructed plasmid pks13-pET-28b was co-transformed with sfp-pET-21b into *E. coli* strain BL21 (DE3). The bacteria containing these recombinant plasmids were grown at 310 K in M9 medium (6 g/L Na_2HPO_4, 3 g/L KH_2PO_4, 1 g/L NH_4Cl, 0.5 g/L NaCl, 0.4% glucose) supplemented with 0.05 g/L kanamycin and 0.1 g/L ampicillin. When the OD600 reached 0.5, the medium was supplemented with amino acids (0.1 g/L L-lysine, L-phenylalanine, L-threonine; 0.05 g/L L-isoleucine, L-leucine, L-valine; and 0.1 g/L L-Se-methionine). In addition, the protein was overexpressed after the addition of 0.3 mM IPTG at 289 K for approximately 16 h. Cell pellets were harvested by 4,000 rpm centrifugation for 10 min and suspended in a solution of 1 mM PMSF, 150 mM NaCl, 25 mM Tris/HCl pH 8.0 suspension buffer. After sonication, we clarified the cell lysate by centrifugation at 15,000 g for 30 min. The supernatant containing the modified protein was applied to a nickel-affinity column (Ni-NTA; GE Healthcare) pre-equilibrated with suspension buffer.

The resin was gradient washed with ice-cold washing buffer (25 mM Tris/HCl pH 8.0, 150 mM NaCl) containing 20, 30, and 40 mM imidazole, and the proteins were eluted with elution buffer (25 mM Tris–HCl pH 8.0, 150 mM NaCl, 250 mM imidazole). Before loading onto the anion exchange column (Source Q; GE Healthcare), the eluate with 250 mM imidazole was diluted half and half with buffer A (25 mM Tris/HCl pH 8.0, 3 mM DTT). Subsequently, the peak fractions were collected for further purification by size-exclusion chromatography (Superdex 200 10/300; GE Healthcare) in 10 mM Tris/HCl pH 8.0 buffer containing 100 mM NaCl. The purity of the protein was identified by 12% SDS-PAGE gels stained by Coomassie brilliant blue. The eluted protein was concentrated by a 10 kDa centrifugal filter and flash-frozen in liquid nitrogen for crystallization.

Crystallization

The protein encoded by the constructed plasmid and labeled with Se-Met was concentrated to 12 mg/ml. Index (Hampton Research) and PEG/ION (Hampton Research) kits were used for the initial crystallization trials at 293 K by the sitting-drop vapor-diffusion method **(Luft et al., 1995)**. Each drop contained 1 µL of protein solution and an equal volume of reservoir solution. The initial crystal was obtained in a solution of 300 mM KAc, pH 8.1 and 20% PEG 3,350. Further crystal optimization experiments were performed by systematic variation of the precipitant concentration. Ultimately, the best crystals were screened in a solution consisting of 300 mM KAc, pH 8.1 and 25% PEG 3,350. The crystals grew to full size in 10 days and were flash-frozen in liquid nitrogen with 10% glycerol added as a cryo-protectant before X-ray diffraction.

Data collection

X-ray diffraction data were collected at 100 K using a Pilatus3 6M detector. All the datasets were obtained at beamline BL19U1 of the Synchrotron Radiation Facility in Shanghai **(Wang et al., 2015)**. A total of 360 images were recorded with 0.5 s exposure at a crystal-to-detector distance of 450 mm, and a total rotation range of 360 was covered using 1.0 oscillation.

Protein N-terminal sequence based on mass spectrum

Regarding the dataset of the crystalized pks13, the initial trial seems not to solve the structure with the whole residues because of lacking density of plentiful residues. The crystals after diffraction by the X-ray were collected together and analyzed with SDS-PAGE stained by Coomassie brilliant blue. The gel with a single low molecular line was processed with the standard In-gel digestion for mass spectrometric to identify the actual location of the degraded fragment in Pks13 (**Shevchenko et al., 2006**).

Data refinement

All datasets were processed by HKL-2000 **(Brodersen et al., 2000)**. The crystal structure of the motif was solved by SAD (Single-wavelength anomalous dispersion） phasing using anomalous data collected on a Se-Met crystal. The final model was manually built in Coot **(Emsley et al., 2010)** and refined in PHENIX **(Adams et al., 2010)**. Final models were validated by Molprobity and deposited in the Protein Data Bank (PDB 5XUO).

Results

Purification and crystallization of Pks13

The full-length Pks13 protein was successfully overexpressed in *E. coli* BL21 (DE3), and the initial crystal condition (300 mM KAc, pH 8.1 and 20% PEG 3,350) was screened. The mature lump-like crystals were optimized after a series of crystal optimization experiments including crystallization with different detergents and additives.

Data collection

X-ray diffraction datasets for the Se-Met-labeled crystals were obtained at beamline BL19U1 of the Synchrotron Radiation Facility in Shanghai with a wavelength of 0.97852 Å. Diffraction images for the crystals were processed using HKL-2000.

Protein N-terminal sequence

The prepared gel was digested by trypsin, and the digestion was purified in to freeze-dried peptide powder. Then the peptide was resolved into the Orbitrap Elite LC-MS/MS for analyzation. The sequenced peptides were blasted within the full-length pks13 protein and the crystalized fragment protein was located ranging from 717aa to 826aa. (Table 2)

Data refinement

The crystal belonged to the space group R32, with asymmetric unit cell parameters of a=93.694, b=93.694, c=97.908, α=β=90, and γ=120. Additionally, the phases were determined by the SAD method. The final model was manually built in Coot and refined in PHENIX to an R_{free} of 26.05% with good stereochemistry. The collected and processed data are presented in Table 3.

Overall Structure of the core motif

The overall structure of the core motif (Fig. 2A) contains a long α helix, five short α helixes and two short η turns, in the order of α1- α2- α3- α4- η1- η2– α5- α6, which constitutes a compact motif. The long α helix, α4, distributes in the midst and is surrounded by the other five short α helixes and two short η turns. The electrostatic potential surface of the core motif also suggests a compact structure (Fig. 2B). Superimposition with the reported structure of the AT domain (PDB code 3tzz) **(Bergeret et al., 2012)**, the core motif was located in the central region of the AT domain (Fig. 3B). The crystallized core motif ranging from 717 to 826 represents approximately one third of the AT domain. Although the structure based on sequence alignment between the core motif and the AT domain shows 100% identity, the secondary structure element presents a

slightly conformational change from 796 to 800, for which refined to two η turns instead of a β strand highlighted by red dash square line (Fig. 3A). The structural alignment performed by SSM in Coot **(Emsley et al., 2004)** shows that the superimposition of the core motif and the AT domain with an rmsd of 1.33Å (Fig. 3C). There are six-stranded β-sheets (β13-β12-β4-β5-β10-β11) in the reported AT domain, while only the central β-strand, β5, is presented in the motif structure, while the C-terminal end has refined as a different element (Fig. 4A). In addition, the AT domain structure in 3tzz, there was a substrate bound to the side of the core motif (Fig. 4C).

Discussion

The overall structure of the core motif of the AT domain is similar to the corresponding part of the reported AT domain, with slight conformational differences (Fig. 4B). The novel structure formed by these bundles seems more tightly packed than the AT domain, especially reflected on the long α4 helix (Fig. 3C). The absence of an appropriate substrate besides the cave of the AT domain probably contributes to a disordered state of these bundles, which might explain the degradation of the full-length Pks13 protein to a fragment.

Importantly, some conserved residues showed a completely different secondary structure. Residues A796, V797, I798, G799, Q800, and S801 formed a β strand in the previously reported AT domain (PDB code 3tzw), which refined as a flexible loop conformation in the motif structure, indicating a more stable state of the whole AT domain when complexed with a substrate (Figure 4B). Comparing to the typical structure of the whole AT domain, a six-stranded β sheet, a speculation was inclined to an unintended degradation that the core motif lacking the substrate became more flexible.

In short, the core motif of the AT domain suggested the inability to absorb a substrate and a tighter packing structure. The disordered structure of the conserved residues located at the C-terminal domain might support the hypothesis that the crystalized structure currently was another crystal packing state of the AT domain. This work provides a new insight into the core motif of AT domain. Our work also provides a structural basis for protein engineering.

Conclusion

The synthesis and transport pathways of mycolic acids in *Mtb* have been a critical drug target. Many biochemical and structural studies have sought to elaborate on the participation of Pks13 in the lipid complex. Obtaining the structure of Pks13 is of great significance in drug screening, as many inhibitors have been reported to target Pks13 or its individual domains (**Aggarwal et al., 2017**).

In this work, we have determined the 2.59 Å high-resolution crystal structure of a partial AT domain from the *Mtb* Pks13 protein. The lack of an appropriate substrate binding to the side cave leads to an unstable and loose state of these bundles, which might explain why it is difficult to obtain the structure of the whole AT domain or the full-length Pks13 protein under the similar screening conditions.

However, the overall structure of Pks13 is still unrevealed, and its mechanism is completely clear. More work should be done, and we hope that our present work will provide some assistance.

Acknowledgments: We gratefully acknowledge the assistance of the staff of BL19U1 at the Shanghai Synchrotron Radiation Facility (SSRF) for their assistance with X-ray diffraction data collection.

References

Abrahams KA, Besra GS. 2016. Mycobacterial cell wall biosynthesis: a multifaceted antibiotic target. *Parasitology* 1-18

Adams PD, Afonine PV, Bunkoczi G, Chen VB, Davis IW, Echols N, Headd JJ, Hung LW, Kapral GJ, Grosse-Kunstleve RW, McCoy A., Moriarty NW, Oeffner R, Read RJ, Richardson DC, Richardson JS, Terwilliger TC, Zwart PH. 2010. PHENIX: a comprehensive Python-based system for macromolecular structure solution. *Acta Crystallographica Section D, Biological Crystallography* **66**: 213-221

Aggarwal A, Parai MK, Shetty N., Wallis D, Woolhiser L, Hastings C, Dutta NK, Galaviz S, Ramesh C. Dhakal RC, Shrestha R, Wakabayashi S, Walpole C, Matthews D, Floyd D, Scullion P, Riley J, Epemolu O, Norval S, Snavely T, Robertson GT, Rubin EJ, Ioerger TR, Sirgel FA, Merwe R, Helden

PD, Keller P, Bottger EC, Karakousis PC, Lenaerts AJ, Sacchettini JC. 2017. Development of a novel lead that targets M.tuberculosis polyketide synthase 13. *Cell* **170**: 249-59. e25

Bergeret F, Gavalda S, Chalut C, Malaga W, Quemard A, Pedelacq JD, Daffe M, Guilhot C, Mourey L, Bon C. 2012. Biochemical and structural study of the atypical acyltransferase domain from the mycobacterial polyketide synthase Pks13. *the Journal of Biological Chemistry* **287**: 33675-90

Bhatt A, Molle V, Besra GS, Jacobs WR Jr.,Kremer L. 2007. The Mycobacterium tuberculosis FAS-II condensing enzymes: their role in mycolic acid biosynthesis, acid-fastness, pathogenesis and in future drug development. *Molecular Microbiology* **64**:1442–1454

Brennan PJ, Nikaido H. 1995. The Envelope of Mycobacteria. *Ann Rev of Bio* 64,29-63

Brodersen DE, Fortelle EL, Vonrhein C, Bricogne G, Nyborg J, Kjeldgaard M. 2000. Applications of single-wavelength anomalous dispersion at high and atomic resolution. *Acta Crystallographica Section D, Biological Crystallography* **56**: 431-41

Chalut C, Botella L, de Sousa-D'Auria C, Houssin C, Guilhot C. 2006. The nonredundant roles of two 4 -phosphopantetheinyl transferases in vital processes of Mycobacteria. *Proceedings of the National Academy of Sciences* **103**: 8511– 8516

Dubey VS, Sirakova TD, Kolattukudy PE. 2002. Disruption of msl3 abolishes the synthesis of mycolipanoic and mycolipenic acids required for polyacyltrehalose synthesis in Mycobacterium tuberculosis H37Rv and causes cell aggregation. *Molecular Microbiology* **45**: 1451–1459

Dubnau E, Chan J, Raynaud C, Mohan VP, LaneÂelle MA, Yu K, QueÂmard A, Smith I, DaffeÂ M. 2000. Oxygenated mycolic acids are necessary for virulence of Mycobacterium tuberculosis in mice. *Molecular Microbiology* **36(3)**:630-637

Emsley P, Cowtan K. 2004. Coot: model-building tools for molecular graphics. *Acta Crystallographica Section D, Biological Crystallography* **60**: 2126-2132

Emsley P, Lohkamp B, Scott WG, Cowtan K. 2010. Features and development of Coot. *Acta Crystallographica Section D, Biological Crystallography* **66**: 486-501

Gavalda S, Le ́ger M, Rest B, Stella A, Bardou F, Montrozier H, Chalut C, Burlet-Schiltz O, Marrakchi H, Daffe M, Que ́mard A. 2009. The Pks13/FadD32 crosstalk for the biosynthesis of mycolic acids in Mycobacterium tuberculosis. *the Journal of Biological Chemistry* **284**: 19255–19264

Herbst DA, Jakob RP, Zahringer F, Maier T. 2016. Mycocerosic acid synthase exemplifies the architecture of reducing polyketide synthases. *Nature* **531**: 533-7

Luft JR, DeTitta GT. 1995. Chaperone salts, polyethylene glycol and rates of equilibration in vapor-diffusion crystallization. *Acta Crystallographica Section D, Biological Crystallography* **51**: 780-5

North EJ, Jackson M, Lee RE. 2014. New approaches to target the mycolic acid biosynthesis pathway for the development of tuberculosis therapeutics. *Current Pharmaceutical Design* **20**: 4357-78.

Portevin D, Sousa-D'Auria C, Houssin C, Grimaldi C, Chami M, Daffe M, Guilhot C. 2004. A polyketide synthase catalyzes the last condensation step of mycolic acid biosynthesis in mycobacteria and related organisms. *Proceedings of the National Academy of Sciences* **101**: 314–319

Shevchenko A, Tomas H, Havlis J, Olsen JV, Mann M. In-gel digestion for mass spectrometric characterization of proteins and proteomes. Nature Protocols, 2006, **1(6)**:2856-60.

Thanna S, Knudson SE, Grzegorzewicz A, Kapil S, Goins CM, Ronning DR, Jackson M, Slayden RA, Sucheck SJ. 2016. Synthesis and evaluation of new 2-aminothiophenes against Mycobacterium tuberculosis. *Organic & Biomolecular Chemistry* **14**: 6119-33

Wang QS, Yu F, Huang S, Sun B, Zhang K, Liu K, Wang ZJ, Xu CY, Wang SS, Yang LF. 2015. The macromolecular crystallography beamline of SSRF. *Nuclear Science and Techniques* **26**: 8-13.

Wilson R, Kumar P, Parashar V, Vilcheze C, Veyron-Churlet R, Freundlich JS, Barnes SW, Walker JR, Szymonifka MJ, Marchiano E, Shenai S, Colangeli R, Jacobs WR, Neiditch MB, Kremer L, Alland D. 2013. Antituberculosis thiophenes define a requirement for Pks13 in mycolic acid biosynthesis. *Nature Chemical Biology* **9:** 499-506

WHO. 2015. Global Tuberculosis Report 2015. 20th ed. Available from: apps.who.int/iris/bitstream/10665/191102/1/9789241565059_eng.pdf.

Figure 1

The overall Pks13 domain structure has the order ACP-KS-AT-ACP-TE.

A. The leading domain N-ACP (25-91) is labelled as orange. The medial threes are mandatory PKS domains, including the KS domain (118-539), the AT domain (715-1018) and the C-ACP domain (1241-1304), labelled as gray, green and orange respectively. The TE domain (1470-1727) is located in the C terminal and labelled as blue. Residues numbers are given below for each domain boundaries. B. The motif locates in the AT domain ranging from 717 to 826. The whole structure is composed of 5 α helixes and 2 short η turns, in the order of N terminal-α1-α2-α3-α4-η1-η2-α5-α6-C terminal.

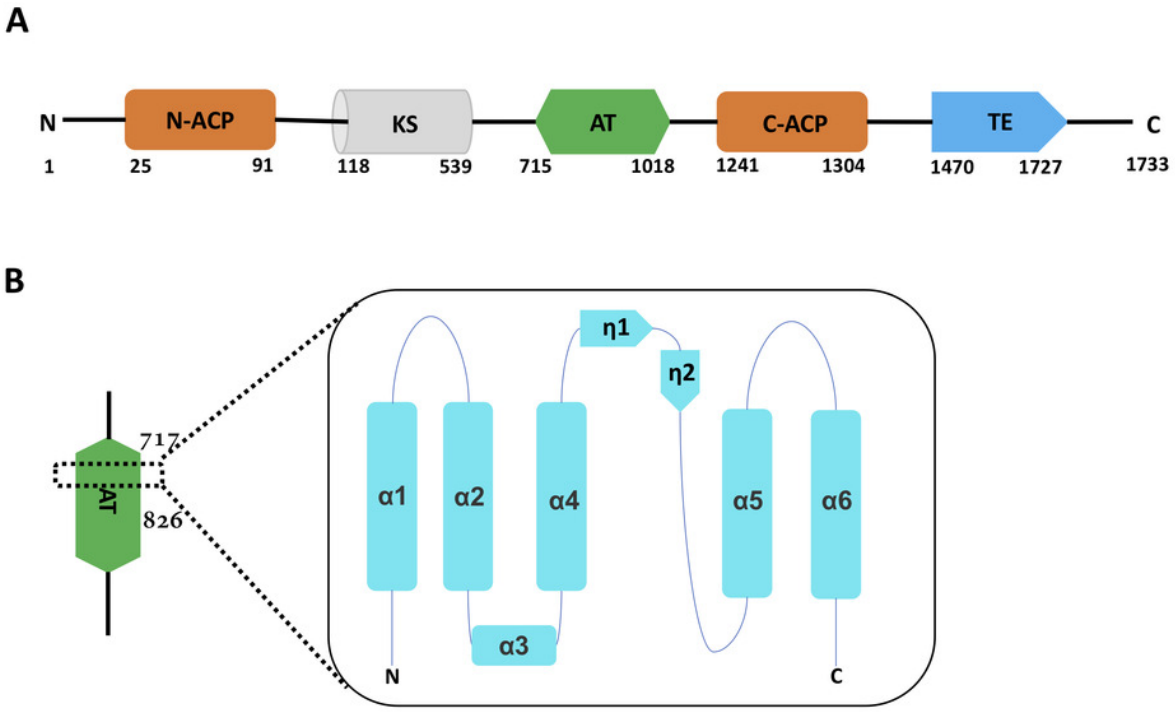

Figure 2

The architecture of the core motif from AT domain.

A. The overall topological structure of the core motif contains a long α helix in the midst, five short α helixes and two short η turns around the long helix, which constitutes a compact motif. Top and down views with a rotation of 90° are exhibited on the right. B. The surface representation is generated by Pymol and colored according to its electrostatic potential (positive potential, blue; negative potential, red).

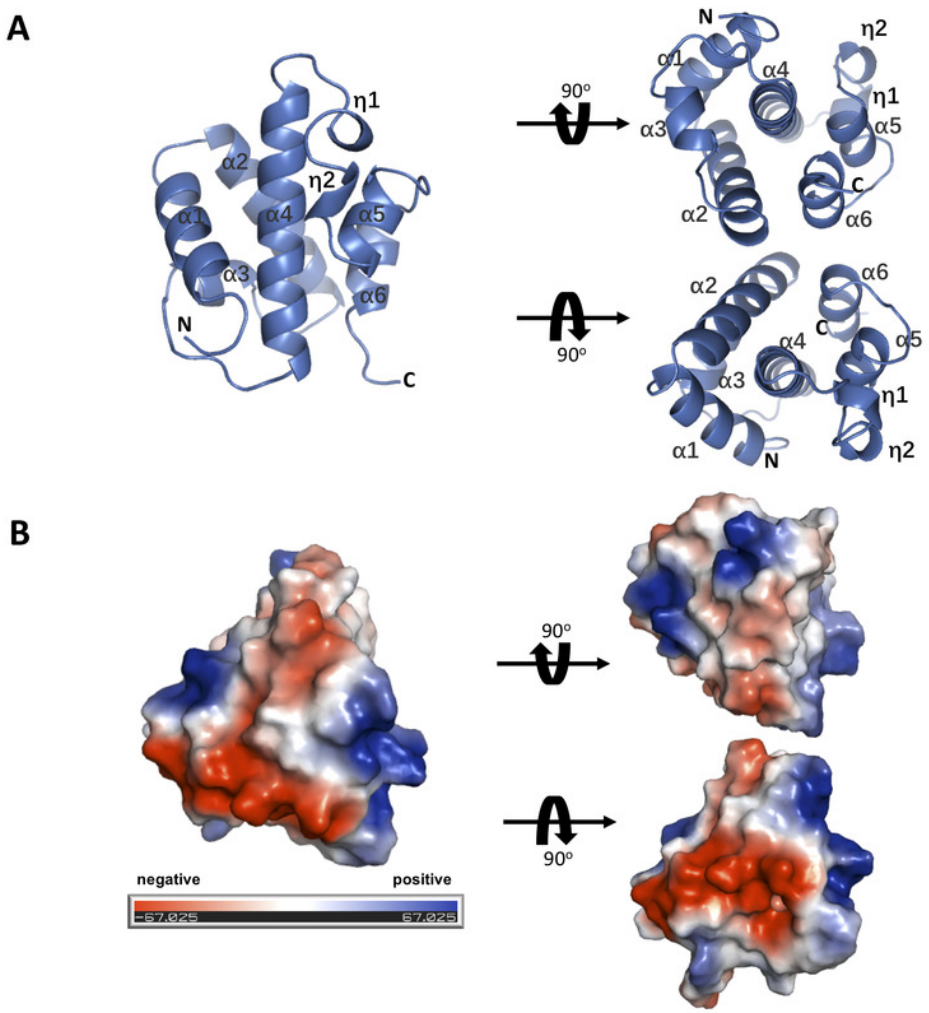

Figure 3

Structural and sequence alignments.

A. structure-based sequence alignment with the whole AT domain. The secondary structural elements of the motif is given along the top of the alignment, below shows the secondary elements belongs to the AT domain (PDB code, 3tzz). The difference between the structures is circled by red dashed line. B. structures of the motif and the AT domain (PDB code, 3tzz) are superimposed together and colored in blue and gray . The region aligned is zoomed in for clear observation. C. The superimposition of the motif and the region could be aligned of AT domain shown in two orthogonal views. The secondary elements are labelled in the picture.

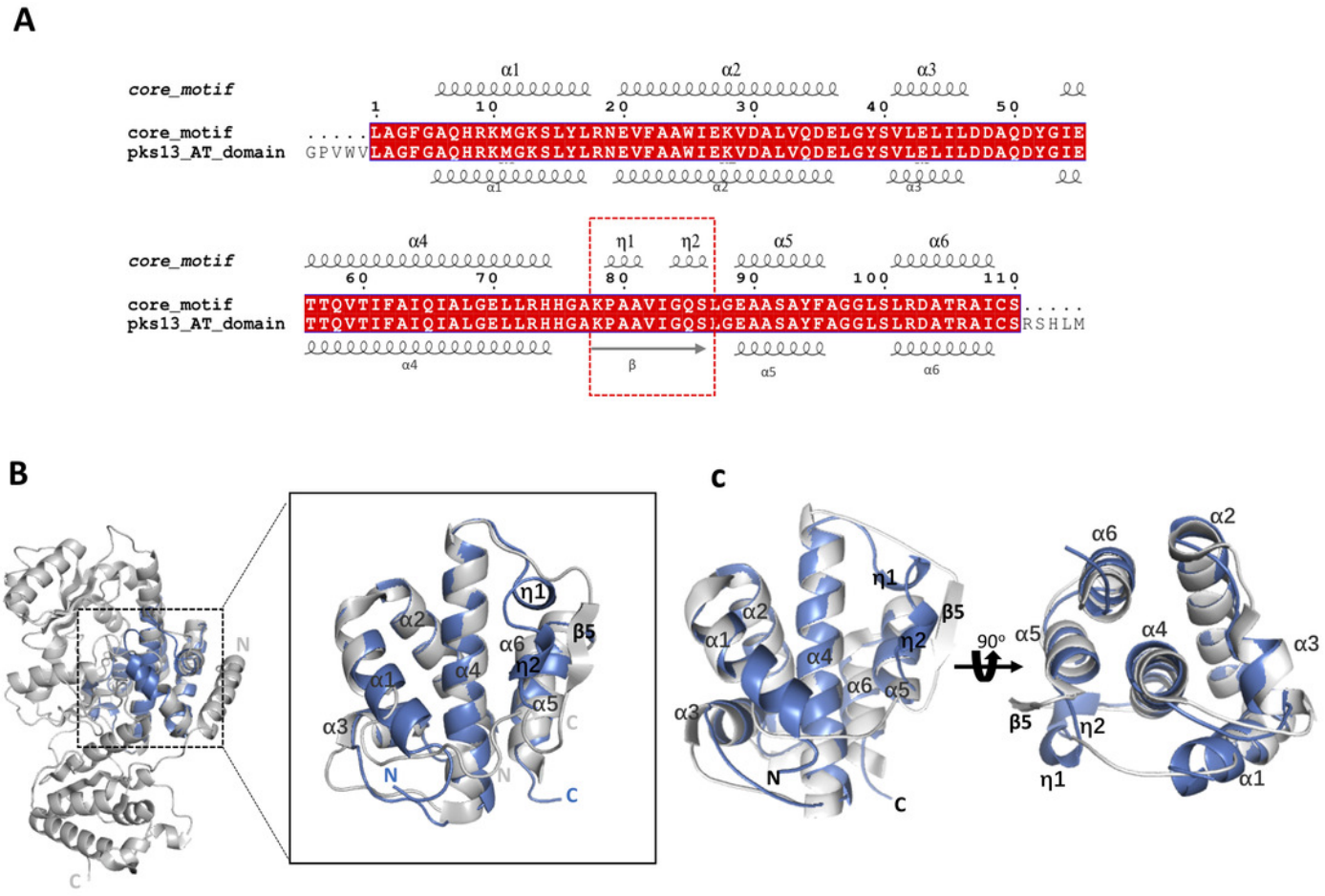

Figure 4

Structural comparison between different states of AT domain.

(A) comparison between the core motif and the whole AT domain (PDB code 3tzw). A tighter packing state was indicated in the figure; (B) some conserved residues formatted a totally different secondary structure, residues K793, P794, A795, A796, V797, I798, G799, Q800, S801 showed as sticks.

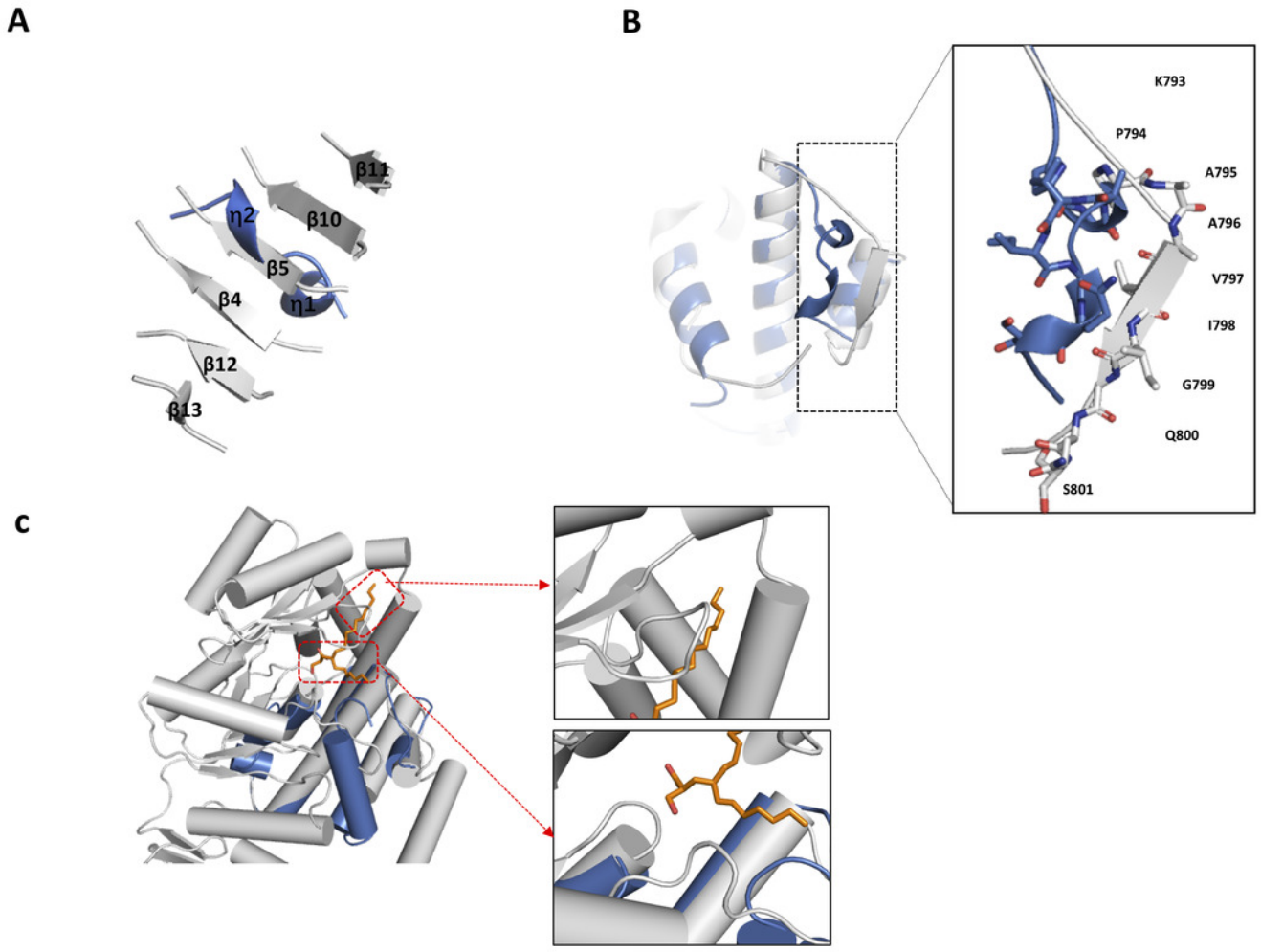

Table 1(on next page)

Macromolecule production information

1

2 Table 1 Macromolecule production information

Source organism	*Mycobacterium tuberculosis*(H37Rv)	*Bacillus subtilis str.168*
DNA source	Full-length Pks13	Sfp (PptT)
Forward primer	5-ggaattccatatgatggcagatgtggccg-3	5-ggaattccatatgaagatttacggaa -3
Reverse primer	5-ccgctcgagctgtttaccaacctcg-3	5-ccgctcgagtcaagcggaagcgata-3
Cloning vector	pET-28b	pET-21b
Expression vector	pET-28b	pET-21b
Expression host	*E. coli* strain(DE3)	*E. coli* strain(DE3)
Complete amino acid sequence of the construct produced	MADVAESQENAPAERA……IEADRTSEV GKQLE	MKIYGIYMDRPLSQEENERF MSFISPEKREKCR……PGYK MAVCAAHPDFPEDITMVSY EELL

3

4

Table 2(on next page)

Mass spectrum based on protein N-terminal sequencing

PEP, Posterior Error Probability of the identification. This value essentially operates as a p-value, where smaller is better.

1 Table 2 Mass spectrum based on protein N-terminal sequencing

Sequence	Length	Mass	Charges	PEP	Score
AGFGAQHR	8	842.9	2;3	0	201.07
AGFGAQHRK	9	971.07	3	0.020363	8.308
HHGAKPAAVIGQSLGEAASAYFAGGLSLR	29	2835.478	2;3;4;5	2.88E-48	83.418
HHGAKPAAVIGQSLGEAASAYFAGGLSLRDATR	33	3278.6909	3;4;5	0.012023	14.817
KMGKSLYLR	9	1094.627	2;3	0.0011449	41.427
MGKSLYLR	8	966.53207	2	5.16E-09	75.109
MGKSLYLRNEVFAAWIEK	18	2154.1296	3;4	1.24E-11	40.856
NEVFAAWIEK	10	1205.6081	2	8.84E-19	89.08
PAAVIGQSLGEAASAYFAGGLSLR	24	2305.2066	2;3	1.27E-303	269.26
PAAVIGQSLGEAASAYFAGGLSLRDATR	28	2748.4195	3	6.29E-159	160
SLYLRNEVFAAWIEK	15	1837.9727	2;3	7.27E-68	127.02
SSGLVPR	7	714.40244	2	3.61E-08	74.191

2

3

Table 3(on next page)

X-ray data collection and refinement statistics

1

2

3 Table 3. X-ray data collection and refinement statistics.

Data Set	Core motif of AT domain
Data collection	
X-ray source	SSRF BEAMLINE BL19U1
Space group	R32
Wavelength(Å)	0.97852
Resolution Range(Å)	50-2.587
Total No. of reflections	90229
No. of unique reflections	5358(524)
Completeness (%)	99.70
Redundancy	16.999
$R_{r.i.m.}$	0.026
$I/\sigma(I)$	41.27(2.10)
Refinement	
Resolution range	50-2.59
Reflections: working/test	5083/276
Final R_{cryst}	23.69%

Final R_{free}	26.05%
rotamer outliers	2.4%
Ramachandran plot:	
favored/allowed/outliers (%)	93.58/4.59/1.83
Rmsd bonds(Å)	0.003
Rmsd angles (°)	0.540
PDB accession code	5XUO